Materials Research Proceedings **4** (2018) 149-154 doi: http://dx.doi.org/10.21741/9781945291678-23

Neutron Transmission Strain Measurements on IMAT: Residual Strain Mapping in an $AlSiC_p$ Metal Matrix Composite

R.S. Ramadhan[1,a*], W. Kockelmann[2,b], A.S. Tremsin[3,c] and M.E. Fitzpatrick[1,d]

[1]Centre for Manufacturing & Materials Engineering Coventry University, Coventry, CV1 2JH, UK

[2]STFC, Rutherford Appleton Laboratory, ISIS Facility, Chilton, OX11 0QX, UK

[3]Space Science Laboratory, University of California at Berkeley, CA 94720 Berkeley, USA

[a]ramadhar@uni.coventry.ac.uk, [b]winfried.kockelmann@stfc.ac.uk, [c]ast@ssl.bekeley.edu, [d]ab6856@coventry.ac.uk

Keywords: Neutron Transmission, Residual Strain, Strain Mapping, Metal Matrix Composite

Abstract. Neutron transmission strain measurements were performed for the first time at the IMAT beamline, ISIS, UK, in order to demonstrate the capability and measure the accuracy of the new instrument. A novel Bragg edge strain analysis technique based on cross correlation is introduced as an alternative to a Bragg edge fitting technique. Neutron transmission measurements were performed on an $AlSiC_p$ metal matrix composite, and the result is compared with the neutron diffraction result on an identical sample, showing good agreement between the two. The advantage of using the proposed cross correlation Bragg edge strain analysis technique over edge fitting is discussed.

Introduction

This paper reports the first attempt of neutron transmission strain analysis at IMAT (Imaging and Material Science), a new, combined imaging and diffraction instrument at the ISIS neutron spallation source, UK [1]. An AlSiCp metal matrix composite (MMC) was chosen as the sample of interest. The sample has a well-characterized residual strain profile, since a similar MMC sample has been previously measured using neutron diffraction [2], and therefore is an ideal test case to provide the level of accuracy of strain measurements on IMAT.

This paper also introduces a new Bragg edge analysis technique based on cross correlation to extract strain information from recorded neutron transmission signals. Until present day, the strain analysis is performed by determining the position of the Bragg edges using a non-linear fitting function. There are several different fitting functions available to describe Bragg edge, among them are functions discussed by Santisteban *et al*. [3] and Tremsin *et al*. [4]. Using the proposed cross correlation technique, the difference of position between any two Bragg edges (i.e. Bragg edge of sample and the reference) can be measured without the need of fitting the Bragg edge itself. The cross correlation technique could be beneficial to measure strain in the presence of texture, where a Bragg edge shape produced by the sample is distorted and difficult to describe with an analytical function.

Experimental

Materials and Specimens. The $AlSiC_p$ MMC sample is composed of Al 2124 matrix and pure silicon carbide particulate. The composite plate was made by evenly mixing 45 μm aluminum alloy powder and 3 μm silicon carbide powder, at 20 % weight fraction, then followed by complicated process including hot isostatic pressing, forging, rolling, cold water quenching and prolonged aging. Such heat treatment is expected to have introduced a parabolic residual strain variation through the thickness of the plate. The dimension of the sample is 35 mm × 35 mm ×

Materials Research Proceedings **4** (2018) 149-154 doi: http://dx.doi.org/10.21741/9781945291678-23

15 mm. The sample used in this study is a section taken from the same MMC plate used in the study by Fitzpatrick *et al*. [2]. Powders of the aluminum matrix and silicon-carbide reinforcement were used as stress-free reference samples.

Neutron transmission measurement. The MMC sample was studied using neutron transmission at IMAT, with a setup as illustrated in Fig. 1a. The incident "white neutron beam", with a wavelength energy spectrum ranging from 0.7 – 6.6 Å, impinged onto the sample which was placed a few mm away from the microchannel plates (MCP) detector. The MCP detector consist of a ^{10}B-doped thin plate as neutron-electron convertor followed by a stack of thin plates with micro-pores as electron amplifier, and an array of 2 × 2 Timepix readout chips. Each chip has 55 µm × 55 µm pixels, and the detector provides 512 × 512 pixels in total, and a 28 × 28 mm^2 field of view. With the setup shown in Fig. 1a, the measured strain direction is parallel with the *x*-axis and averaged through the thickness of the sample along the transmission path. The coordinate system is shown in Fig. 1a, and each measurement was performed for 5 hours.

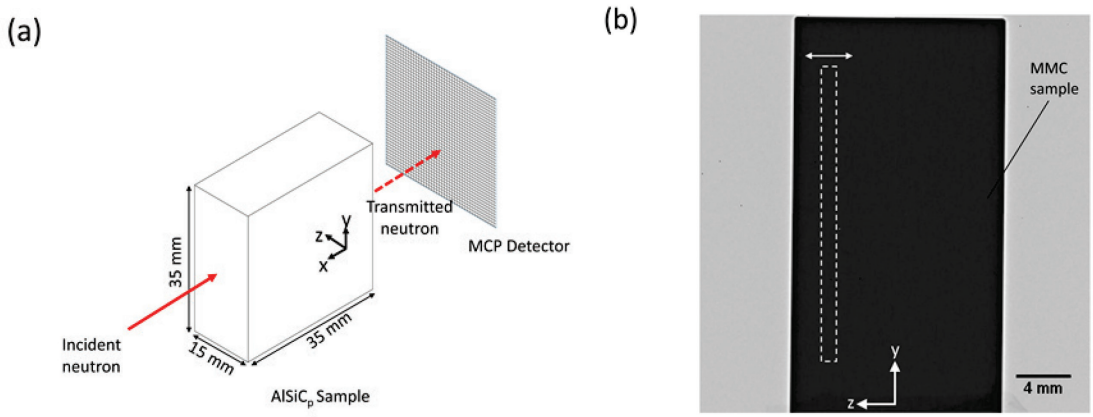

Fig. 1: (a) Setup of neutron transmission measurement; (b) Radiographic image of MMC sample, white dashed line showing averaging area for spatially-resolved strain measurement.

Bragg edge analysis for strain measurements

A Bragg edge, which signifies a sudden increase in neutron transmission, is formed as a consequence of backscattering phenomena [5]. The recorded transmission spectrum of AlSiC$_p$ MMC is shown in Fig. 2a, showing Bragg edges from both the aluminum matrix and the silicon-carbide reinforcement. In this work, two different analysis techniques were used to extract strain information from the Bragg edge signal. The first technique was to determine the strain using the shift in position between single Bragg edge from the sample and stress-free reference. The determination of the Bragg edge position was performed by fitting the measured data using two non-linear fitting functions described by Santisteban *et al*. [3] and Tremsin *et al*. [4], which will be called the Santisteban and Tremsin function, respectively, in the rest of this paper. An example of fitting results using the two fitting functions is shown in Fig. 2b.

The second technique to determine strain is based on applying a cross correlation algorithm between the sample Bragg edge and the stress-free reference Bragg edge data. Cross correlation is a mathematical function to measure similarity between two signals as function of the shift of one relative to the other. The analysis was carried out by initially taking the first derivative of both the sample and reference {111} Bragg edge signal. Then, cross correlation was performed on the two derivatives using Eq. (1):

$$y(m) = \sum_{n=0}^{M-1} f(n)g(n-m) = ifft(FG^*) \quad (1)$$

Materials Research Proceedings **4** (2018) 149-154 doi: http://dx.doi.org/10.21741/9781945291678-23

where f(n) and g(n) are the two Bragg edge derivatives, F is the Fourier transform of f(n), G is the Fourier transform of g(n), * means complex conjugation, ifft stands for inverse fast Fourier transform and y(m) is the correlation output. A Voigt function then is used to fit the peak-shaped correlation curve. The peak of the curve provides the information of position where the two Bragg edges are most similar, and thus inform on the shift (i.e. differences in position) between the edges. The shift is then used to calculate the strain.

Spatially resolved strain data were extracted by fitting the Bragg edges averaged over a region with 1 mm × 20 mm dimension, scanning along the *z*-axis, as shown in radiographic image of the sample, Fig. 1b. The selection area is elongated in *y*-axis direction in order to increase the statistics of the Bragg edge, assuming that there is not much strain variation as function of position along the *y*-axis. Strain mapping was performed by fitting the Bragg edge for all pixels on the dataset, using Tremsin function. Before fitting, neutron counts from several neighboring pixels over 2.2 mm × 2.2 mm area were combined into one spectrum, to improve the statistics [6], and maps were produced with a step size of 55 m using the 'running average' of this box.

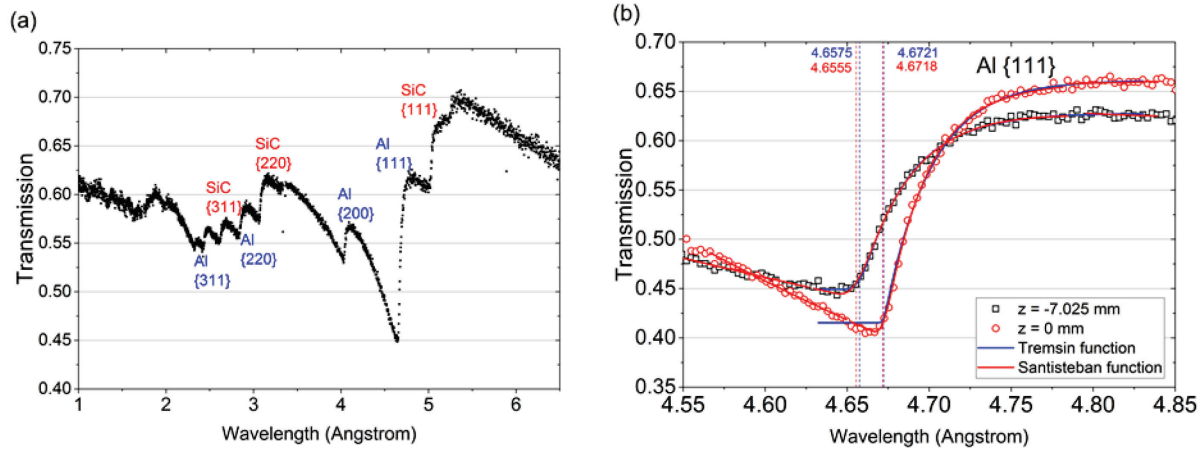

Fig. 2: (a) Transmission spectra of AlSiC$_p$ MMC sample; (b) Fitting of Al {111} Bragg edges for two different regions of interest using Santisteban and Tremsin functions.

Results

Residual strain values for the aluminum matrix of the AlSiC$_p$ MMC are shown in Fig. 3a. A parabolic strain profile through the thickness of the sample can be clearly seen where compressive strain is apparent on both surfaces of the plate, and with tensile strains in the middle. This is expected due to uneven material shrinkage caused by rapid cooling of the quenching process. The Tremsin function consistently gave slightly higher strain values compared to the Santisteban function, Fig. 3. Figure 3b show residual strain values for the silicon-carbide reinforcement component. It can be seen that the scatter of the data from silicon-carbide is higher than it is for aluminum. This is due to both lower levels of strain and a smaller volume fraction of silicon-carbide in the MMC sample that contributes to the Bragg edge signal. Although the measurement result is more scattered, a second-order polynomial fit of the strain measurement shows that the silicon-carbide component also has a parabolic-shaped strain profile, Fig. 3b.

Bragg edge strain analysis based on cross correlation was performed on the same dataset. The result was compared to strain analyzed with the Santisteban function. The strain measured by neutron transmission in this study was then compared with previous literature values measured

Materials Research Proceedings **4** (2018) 149-154 doi: http://dx.doi.org/10.21741/9781945291678-23

by neutron diffraction on the similar MMC sample [2]. The comparison is shown in Fig. 4. In general, the neutron transmission shows very good agreement with the neutron diffraction result. The parabolic strain profile in the aluminum matrix measured by neutron diffraction is replicated almost with the exact magnitude and trend from neutron transmission, Fig. 4a. The strain analyzed by the cross correlation technique shows better agreement with neutron diffraction results. Cross correlation curves also have smaller errors compared to the non-linear fitting function results, Fig. 4a. Similarly, good agreement can be found between neutron diffraction and neutron transmission results for the silicon-carbide reinforcement phase, Fig. 4b. Despite the scatter of the data, neutron diffraction and neutron transmission strain values fall within the same range and follow the same trend.

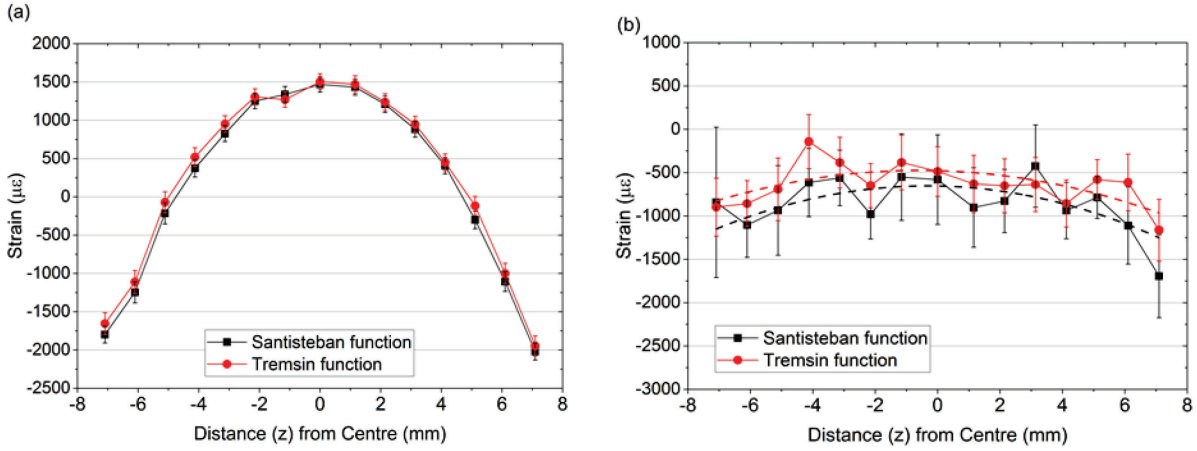

Fig. 3: x-axis residual strain as function of position along z-axis for (a) aluminum matrix and (b) silicon carbide reinforcement component of the $AlSiC_p$ MMC sample.

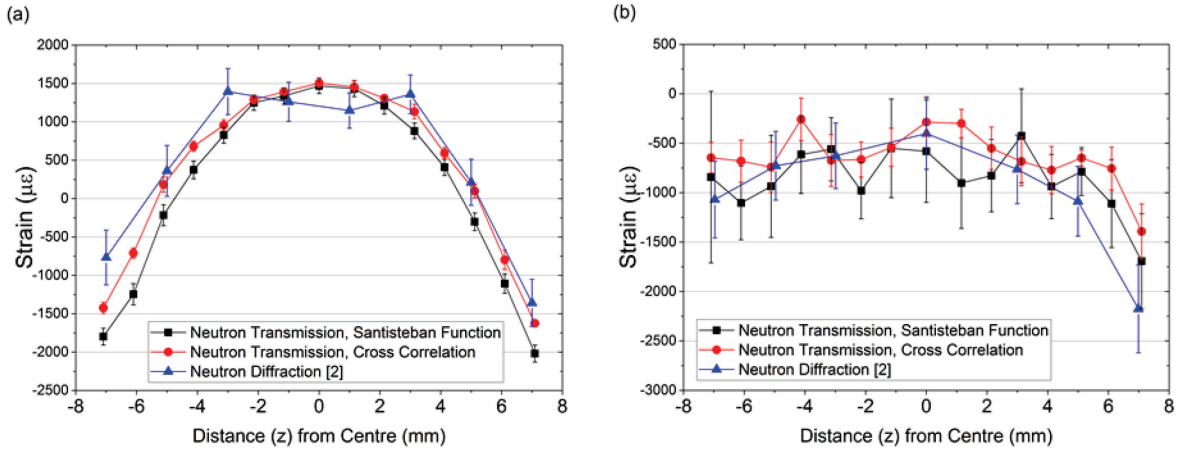

Fig. 4: Comparison between x-axis residual strain profiles obtained from neutron transmission using the non-linear fitting function, neutron transmission using cross correlation analysis, and neutron diffraction [2] for (a) aluminum and (b) silicon carbide component of MMC sample.

Figure 5 shows the reconstructed 2D residual strain maps within the MMC sample. A gradient of strain within the aluminum matrix through the thickness of the plate (*z*-axis direction) can be clearly observed, where compressive strain is apparent on both surfaces accompanied by tensile strain in the middle of the plate, Fig. 5a. Meanwhile, there is no significant strain variation along the *y*-axis direction, Fig. 5a. Figure 5b shows the residual strain map of the silicon-carbide component. The strain gradient through the thickness of the plate is less apparent due to higher

Materials Research Proceedings **4** (2018) 149-154 doi: http://dx.doi.org/10.21741/9781945291678-23

stiffness of silicon-carbide, although regions of tensile strain still can be found in the middle of the plate. Following the data analysis for strain mapping described in [6], the achieved spatial resolution is in range of a few hundred microns.

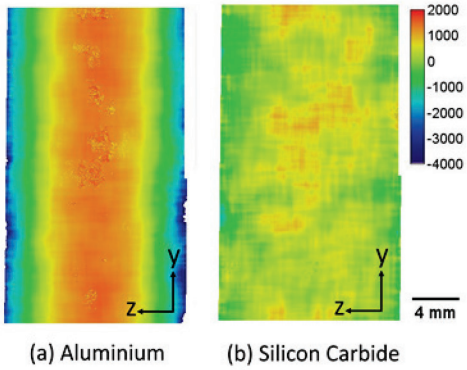

Fig. 5: Residual strain map of $AlSiC_p$ MMC sample measured using neutron transmission.

Discussion

Fitting Bragg edges. Having more parameters to model the data, the Santisteban function can fit the Bragg edge better compared to the Tremsin function, especially for the data on the left hand side of the edge which shows negative exponential function, Fig. 2b. This leads to discrepancies within 190 μstrain between the fitting results, Fig. 3a. The slope of the exponential function on the left hand side of the Bragg edge is often influenced by preferred orientation present in the sample. As many engineering samples have some degree of preferred orientation, the Santisteban function is more robust and should be used for Bragg edge analysis.

Cross correlation. As mentioned above, the shape of a Bragg edge can be affected by the preferred orientation present in the sample. In the case where this texture effect is very strong, the Bragg edge shape is difficult to be modelled by an analytical function. The cross correlation technique proposed in this study eliminates the need of fitting the individual Bragg edges, and therefore theoretically allows strain analysis from Bragg edges of any shape. The early implementation of cross correlation in this study shows that this analysis technique performs as good as non-linear fitting functions. Bragg edge strain analysis using cross correlation and non-linear analytical functions yields comparable trends, with average differences in values less than 400 μstrain, Fig. 4. Moreover, especially for aluminum matrix data, cross correlation results shows better agreement with neutron diffraction, Fig. 4a. This might indicate that cross correlation measured strain more accurately in the presence of texture in the sample. The current limitation of this technique is the inability to analyse data with high noise. Using Eq. 1, cross correlation works better for peak-shaped data, and thus creating the need of performing the technique on the first derivative to the Bragg edge spectra. Consequently, this differentiation process amplifies the noise of the data. Therefore, at this point, the cross correlation works best for analysing statistically-good Bragg edge data.

Strain measurements on IMAT. The agreement between neutron transmission and neutron diffraction results shows the accuracy of IMAT instrument for strain measurement. The difference in values between IMAT results and neutron diffraction results for the sample studied is within ~500 μstrain using the non-linear fitting function technique and ~250 μstrain using the cross correlation technique, Fig. 4. Some of the difference is due to the fact that the neutron diffraction result was taken from a different cut of an identical plate, hence adding to the uncertainty. Also, the neutron transmission averaged the strain variation through the thickness of the sample, while neutron diffraction measured at a specific locations within the sample

thickness. Further studies will be conducted to investigate the accuracy and the resolution of the strain that can be measured at IMAT, whether using a round-robin reference sample [7], or measuring exactly the same sample using both neutron transmission and neutron diffraction. This study also demonstrated the capability of strain mapping on IMAT using the MCP detector. 2D strain maps can provide better understanding of local strain gradients within the sample. In this case it proves the initial assumption that there is not much strain variation along the *y*-axis direction, Fig. 5. Considering the sub-mm spatial resolution that was achieved, IMAT is able to produce the strain map in a relatively short time and in a simple experimental setup.

Conclusion

The capability and accuracy of the IMAT instrument for neutron transmission strain measurements has been demonstrated by the good agreement between neutron transmission and neutron diffraction results on two identical $AlSiC_p$ metal-matrix composite samples. A novel Bragg edge strain analysis based on cross correlation has been introduced, showing agreement within ~250 μstrain with neutron diffraction results. Comparatively, using a commonly used non-linear fitting function, neutron transmission shows agreement within ~500 μstrain with neutron diffraction. Accordingly, the strain mapping capability of IMAT has been demonstrated, and will be advantageous to study samples with more complicated residual strain distributions.

References

[1] T. Minniti, W. Kockelmann, G. Burca, J.F. Kelleher, S. Kabra, S.Y. Zhang, D.E. Pooley, E.M. Schooneveld, Q. Mutamba, J. Sykora, N.J. Rhodes, F.M. Pouzols, J.B. Nightingale, F. Aliotta, L.M. Bonaccorsi, R. Ponterio, G. Salvato, S. Trusso, C. Vasi, A.S. Tremsin and G Gorini, Materials analysis opportunities on the new neutron imaging facility IMAT@ISIS, J. Inst. 11 (2016)

[2] M.E. Fitzpatrick, M.T. Hutchings and P.J. Withers, Separation of macroscopic, elastic mismatch and thermal expansion misfit stresses in metal matrix composite quenched plates from neutron diffraction measurements, Acta Mater. 45 (1997) 4867–4876. https://doi.org/10.1016/S1359-6454(97)00209-7

[3] J.R. Santisteban, L. Edwards, A. Steuwer and P.J. Withers, Time-of-flight neutron transmission diffraction, J. Appl. Crystallogr. 34 (2001) 289–297. https://doi.org/10.1107/S0021889801003260

[4] A.S. Tremsin, J.B. McPhate, W. Kockelmann, J.V. Vallerga, O.H.W. Siegmund and W.B. Feller., Energy-Resolving neutron transmission radiography at the isis pulsed spallation source with a high-resolution neutron counting detector, IEEE Trans. Nucl. Sci. 56 (2009) 2931–2937. https://doi.org/10.1109/TNS.2009.2029690

[5] J.R. Santisteban, L. Edwards, M.E. Fitzpatrick, A. Steuwer, P.J. Withers, M.R. Daymond, M.W. Johnson, N. Rhodes and E.M. Schooneveld, Strain imaging by Bragg edge neutron transmission, Nucl. Instr. Meth. Phys. Res. A 481 (2002) 765–768. https://doi.org/10.1016/S0168-9002(01)01256-6

[6] A.S. Tremsin, T.Y. Yau and W. Kockelmann, Non-destructive Examination of Loads in Regular and Self-locking Spiralock ® Threads through Energy- resolved Neutron Imaging, Strain 52 (2016) 548–558. https://doi.org/10.1111/str.12201

[7] M.R. Daymond, M.W. Johnson and D.S. Sivia, Analysis of neutron diffraction strain measurement data from a round robin sample, J. Strain Anal. 37 (2002) 73–85. https://doi.org/10.1243/0309324021514844